Electronic Supplementary Information

Hierarchical $(Ni,Co)_{0.85}Se$ Sheets for Efficient Oxygen Evolution Reaction Electrocatalysis: A Combined Approach of Fabrication Control and Mechanistic Understanding

Muhammad Sohail Riaz,[‡a] Qi Huang,[‡c] Jingjing Duan,[c] Sheng Chen,[c]* Fuqiang Huang[b]* and Pau Farras[a]*

(a) School of Biological and Chemical Sciences, Energy Research Centre, Ryan Institute, University of Galway, H91 CF50 Galway, Ireland Email: Pau.farras@universityofgalway.ie

(b) State Key Lab of Metal Matrix Composites, School of Materials Science and Engineering, Shanghai Jiao Tong University, Shanghai 200240, China. Email: huangfq@sjtu.edu.cn

(c) Key Laboratory for Soft Chemistry and Functional Materials (Ministry of Education), School of Chemical Engineering, School of Energy and Power Engineering, Nanjing University of Science and Technology, Nanjing, 210094, China. Email: sheng.chen@njust.edu.cn

Experimental Section

Materials: $Co(NO_3)_2{\cdot}6H_2O$ (A.R.), $Ni(NO_3)_2{\cdot}6H_2O$ (A.R.), Na_2SeO_3 (A.R.), absolute ethanol C_2H_5OH (A.R.), and urea (A.R.) were received from Xilong Scientific Company Ltd., China. PVP (K30) and RuO_2 (A.R.) were purchased from Aladdin and Alfa Aesar. Deionized water was used throughout the experiment.

Materials Synthesis:

Synthesis of $Ni_xCo_{2-x}(CO_3)(OH)_2$: Ni doped $Co_{2-x}(CO_3)(OH)_2$ layered sheets were generated in the first step. Briefly, 5 g of PVP (K30), $Ni(NO_3)_2{\cdot}6H_2O$, $Co(NO)_3{\cdot}6H_2O$ (samples with different amounts of Ni doping in Co, i.e., 0 %, 5 %, 10 %, 15 % prepared to keep the total mass at 3 mmol) and urea 20 (mmol) were dissolved in 70 mL distilled water and stirred for 30 minutes, autoclaved at 160 °C in a 100 mL Teflon for different reaction times (1 to 6 hour). The uniform smooth sheets formed within 6 hours of the reaction were used as a precursor in the next step. After cooling, the obtained product was centrifuged 3 to 4 times with a water/ethanol system to remove the surfactant from the precursor surface. The samples dried at 70 °C for 4 hours. The product obtained was identified as $Ni_xCo_{1-x}(CO_3)(OH)_2$ sheets.

Selenization of $Ni_xCo_{1-x}(CO_3)(OH)_2$: In short, 0.2 g of the Ni/Co hydroxide carbonate precursor, 0.6 g of sodium selenite (Na_2SeO_3) dissolved in 50 mL of water and stirred for 30 minutes added 10 mL of $N_2H_4{\cdot}H_2O$ solution dropwise. The mixture was sealed in a hydrothermal vessel and autoclaved for 12 hours at 180

°C. The product obtained through filtration was $(Ni,Co)_{0.85}Se$. The sample was cooled naturally, washed with water and ethanol several times, and dried in an oven at 70 °C for 4 hours.

Materials Characterizations*:* Morphology characterized by transmission electron microscopy (TEM) and selected area electron diffraction (SAED) with a JEM-2100 electron microscope (JEOL Ltd., Japan) working at 200 kV. The Hitachi S-4800 electron microscope accomplished the scanning electron microscope (SEM), operational at 5 kV. N_2 adsorption/desorption isotherm determined by the Brunauer-Emmett-Teller (BET) measurement using an ASAP-2020 surface area analyzer at liquid nitrogen temperature. The pore size distribution (PSD) was attained from the pore size distribution curve's adsorption branch acquired through the Barrett-Joyner-Halenda (BJH) approach. The powder X-ray diffraction (XRD) pattern was obtained on a Bruker D2 with Cu Kα radiation (λ = 1.5418 Å) with a scan rate of 5° min^{-1} in the 2θ range of 10–80°. The X-ray photoelectron spectroscopy (XPS) measurements were done using an Axis Ultra imaging photoelectron spectrometer (monochromatized Al Kα anode, Kratos Analytical Ltd.).

Formation mechanism of micro-sheets and needle-like morphology:

Precursor decomposition and hydroxide carbonate formation is achieved by: nickel nitrate hydrate and cobalt nitrate hydrate dissociate into Ni^{2+} and Co^{2+} ions in the deionized water (DI). Urea ($(NH_2)_2CO$) undergoes thermal decomposition and hydrolysis, but in addition to releasing OH^- ions, it also produces carbonate (CO_3^{2-}) and ammonium (NH_4^+) ions: [1]

$$(NH_2)_2CO + 2H_2O \rightarrow 2NH_4^{+} + CO_3^{2-}$$

This decomposition occurs gradually under hydrothermal conditions (high temperature and pressure).
The released OH^- ions react with Ni^{2+} and Co^{2+} to form the hydroxide component, while the carbonate ions (CO_3^{2-}) interact with these metal ions to form a nickel cobalt hydroxide carbonate phase.

$$xNi^{2+} + yCo^{2+} + CO_3^{2-} + OH^- \rightarrow Ni_xCo_y(OH)_2CO_3$$ (nickel cobalt hydroxide carbonate)

During the early stages of the hydrothermal reaction, the precipitation of Ni-Co hydroxide carbonate results in the formation of *needle-like structures*. These needles may initially consist of small crystallites or nanorods due to anisotropic growth as a result of differential binding of metal ions to various crystal planes. The presence of PVP plays a key role in shaping the growing structures. PVP binds preferentially to certain crystallographic surfaces, stabilizing specific crystal faces and directing anisotropic (one-dimensional) growth, which leads to the needle-like morphology. With increasing time and temperature in the hydrothermal environment, the *needle-like structures* start to transform into 2D sheets. This transformation can occur via one or both of the following mechanisms: i) *Ostwald Ripening:* The smaller needle-like structures dissolve and redeposit as larger, more stable nanosheets. This is driven by the need to minimize surface energy, as the sheet-like morphology has lower surface energy than needle-like shapes[2]. ii) *Oriented Attachment:* Individual primary nanocrystals (forming the needle structures) align and fuse together along specific crystallographic directions, forming extended 2D nanosheets. Hydrothermal conditions and PVP interactions often facilitate the alignment[3]. The carbonate ions (CO_3^{2-}) also play a role in this morphological evolution. Carbonate ions can interact with specific crystal facets, contributing to anisotropic growth that favours 2D sheet formation over 1D needles. PVP acts as a capping

agent, controlling the growth of the Ni-Co hydroxide carbonate particles.[4] It selectively adsorbs onto certain crystal facets, directing the anisotropic growth of the initial needle-like structures. As the needles transform into nanosheets, PVP further stabilizes the 2D morphology by preventing aggregation or uncontrolled growth, allowing the nanosheets to form uniformly. The reaction reaches equilibrium after sufficient time under hydrothermal conditions, and the nickel-cobalt hydroxide carbonate nanosheets become stable. The nanosheets are thermodynamically more stable than the initial needle-like structures due to their lower surface energy. The carbonate ions and PVP help stabilize the final nanosheet structure, preventing further morphological changes or aggregation.[5]

Electrochemical measurement: We made the catalyst ink by mixing acetylene black (1 mg) and catalyst (5 mg) in 1 mL of a 0.5 wt% Nafion/alcohol solution using ultrasonication for 30 minutes and later stirred for 12 hours before measuring electrochemical activity. We used a CHI 760E electrochemical workstation with a three-electrode system for electrochemical measurements. The glassy carbon modified with catalyst ink was used as a working electrode, whereas the Pt wire and Hg/HgO (0.098 V *vs.* SHE, 1M NaOH) were used as counter and reference electrodes in a 0.1M KOH electrolyte. The mass loading of the catalyst on the working electrode is about 255 µg cm^{-2}. The oxygen evolution performance of the catalysts was acquired by cyclic voltammetry (CV). The data was gathered from 0.2 V to 1.0 V (*vs*. Hg/HgO) at a scan rate of 50 mV s^{-1} with a rotating speed of 2000 rpm. We performed the linear sweep voltammetry (LSV) measurements at a scan rate of 10 mV s^{-1}. Electrochemical impedance spectroscopy (EIS) was measured from 0.01 Hz to 100 kHz, with an amplitude of 5 mV. Chronopotentiometry was tested to check the robustness of the catalyst. *iR* correction was performed, and data was standardized to RHE using:

In 0.1 M KOH, E (vs. RHE) = E (vs. Hg/HgO) + 0.098 + 0.0592×pH (pH=13).

Computational Methods: First-principles calculations were performed by the MedeA-Vienna Ab initio Simulation Package (VASP) based on DFT methods[6, 7]. The Perdew-Burke-Ernzerhof (PBE) generalized gradient approach[8, 9] was used to define the exchange-correlation potential. The interaction between the atomic cores and electrons was described using the projector augmented wave method (PAW)[10, 11]. The plane wave energy cutoff was set to be 450 eV. The Brillouin zone in the real space was sampled with a 1×1×1 Monkhorst-PackK-point grid. The convergence criterion was set to be 10^{-5} eV and 0.02 eV/Å for energy and force in the geometry optimizations, respectively. A Gaussian smearing method was employed with 0.1 eV width. Hubbard-U correction method (DFT+U) was carried out to improve the description of highly correlated Co and Ni 3d orbitals with the values of U-J both set to be 2.5 eV[12, 13].

A surface was cleaved across a (101) direction to form a $(Ni, Co)_{0.85}Se$ slab. Intermediates were adsorbed on the surface by the Co-O bond.

The detailed Gibbs free energy calculation for OER has been carried out by putting a portion atom of $(Ni, Co)_{0.85}Se$ into a large cell (26 Å × 16 Å × 11 Å) according to the following equation:

$$G = E + ZTE - TS$$

Where G, E and ZTE refer to chemical potential, electronic energy and zero-point energy, respectively. The entropy can be calculated by the sum of the vibrational, rotational, translational, and electronic contribution as to:

$S = S_v + S_r + S_t + S_e$

Since $S_e \approx 0$ at the fundamental electronic level[14].

For the case of solids and adsorbates, some approximations can be adopted:

Translational and rotational motions can be omitted, therefore, $S_t \approx 0$ and $S_r \approx 0$. In this case, all the entropy values come from the vibrational contribution: $S = S_v$

Finally, Gibbs free energy for different states was calculated as to:

$G = E + ZTE - TS_v$

The following equation calculated the overpotential:

$\eta = {G_{max}}/{e} - 1.23\ V$

Table 1 Performance comparison with the reported catalyst for OER in the same conditions

Catalyst	Overpotential @10 mA cm^{-2} (mV)	Tafel Slope (mV dec^{-1})	Electrolyte	Substrate	References
CoO/Co	350	79.6	0.1 M KOH	Glassy Carbon	15
Co@CoP_x	310	81.7	0.1 M KOH	Glassy Carbon	16
Co_7Ni_3	350	66.7	0.1 M KOH	Glassy Carbon	17
$NiCo_2S_4/Co_9S_8$	320	72.2	0.1 M KOH	Glassy Carbon	1
NiCo Selenide	312	66.0	0.1 M KOH	Glassy Carbon	18
$NiCo_{0.85}$ Se	290	77.4	0.1 M KOH	Glassy Carbon	This work

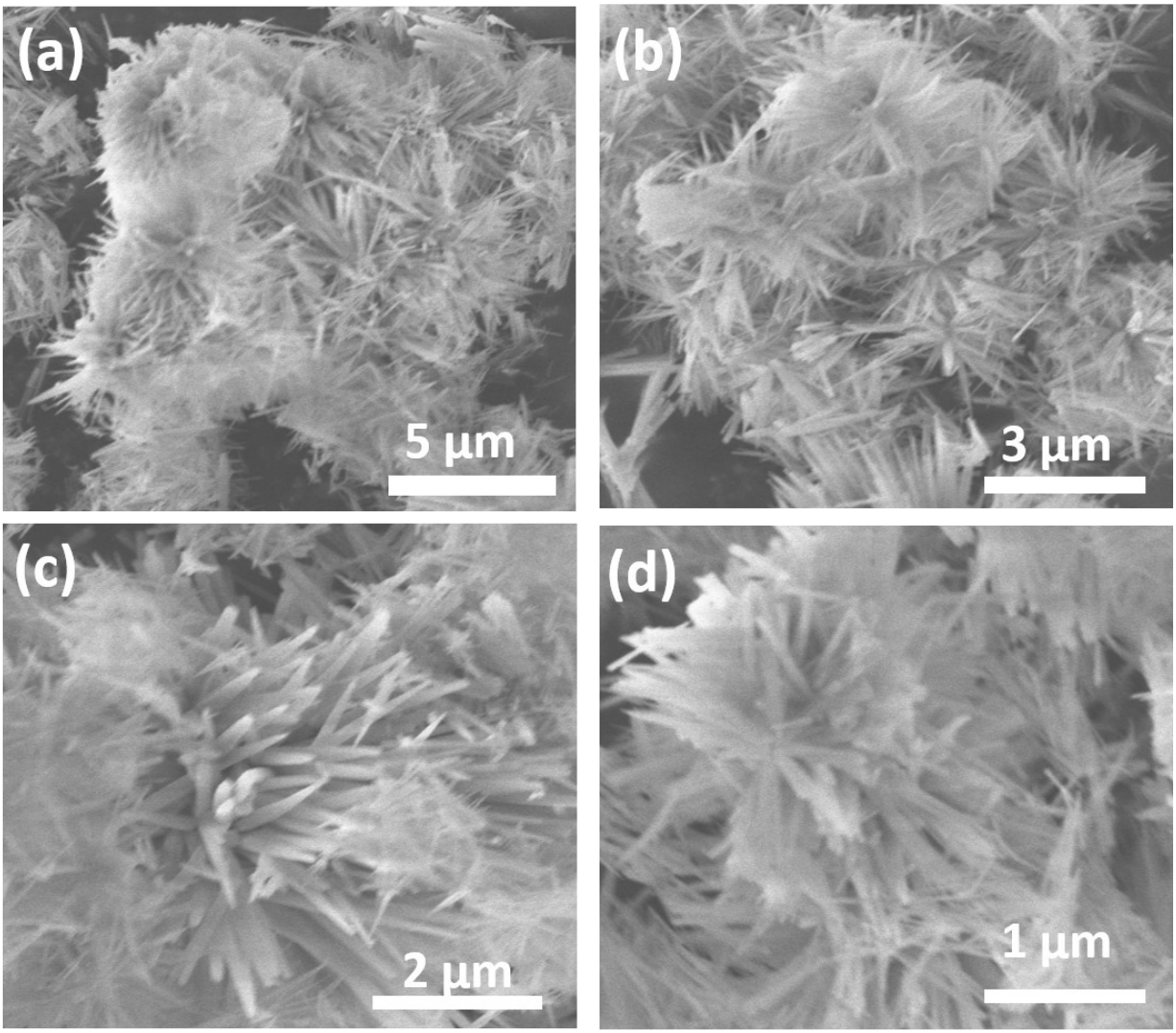

Fig. S1 Scanning Transmission Electron Microscopy images at reaction time equal to 1 hour for $Ni_xCo_{2-x}(CO)_3(OH)_2$

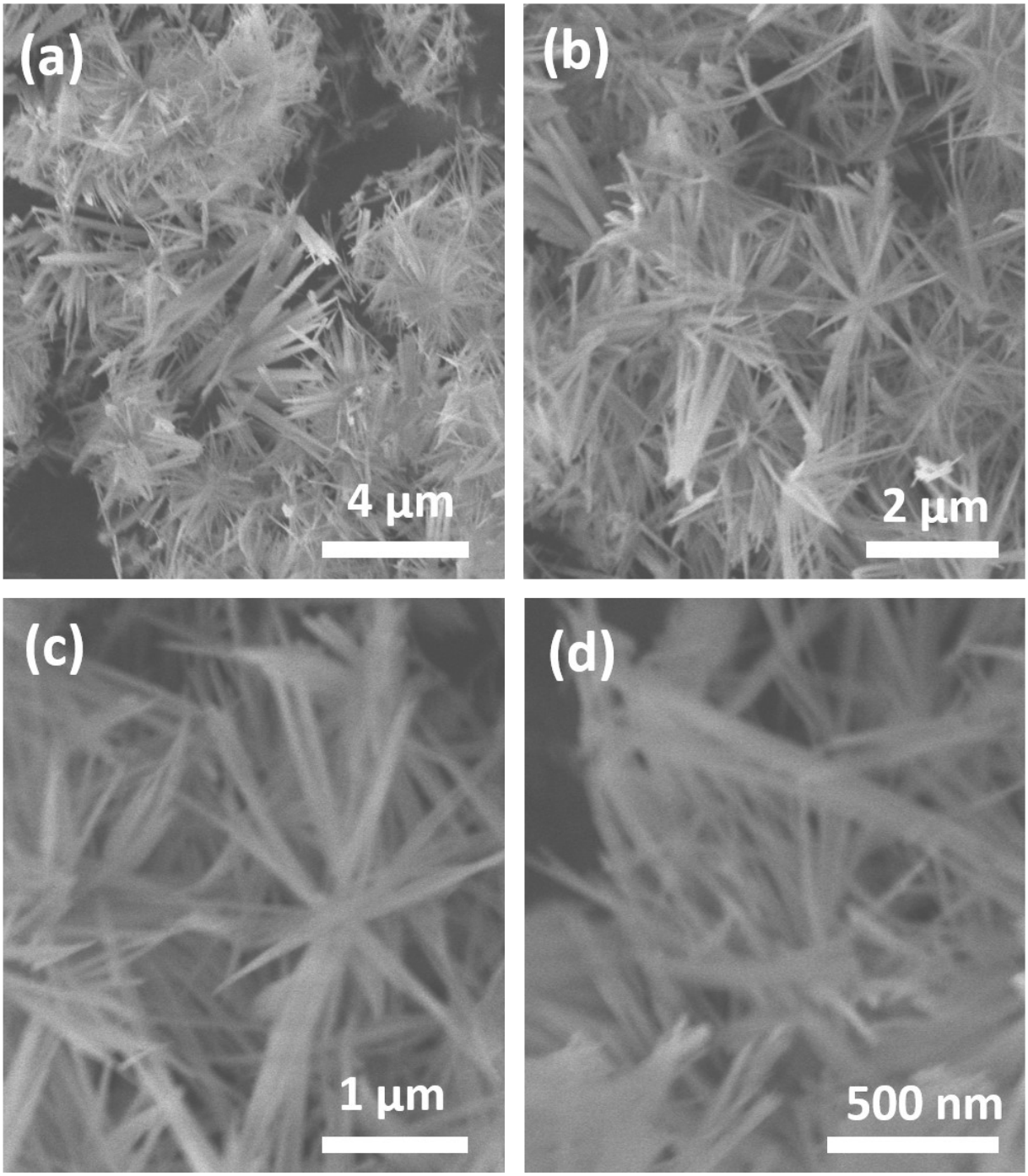

Fig. S2 Scanning Transmission Electron Microscopy images at reaction time equal to 2 hours for $Ni_xCo_{2-x}(CO)_3(OH)_2$

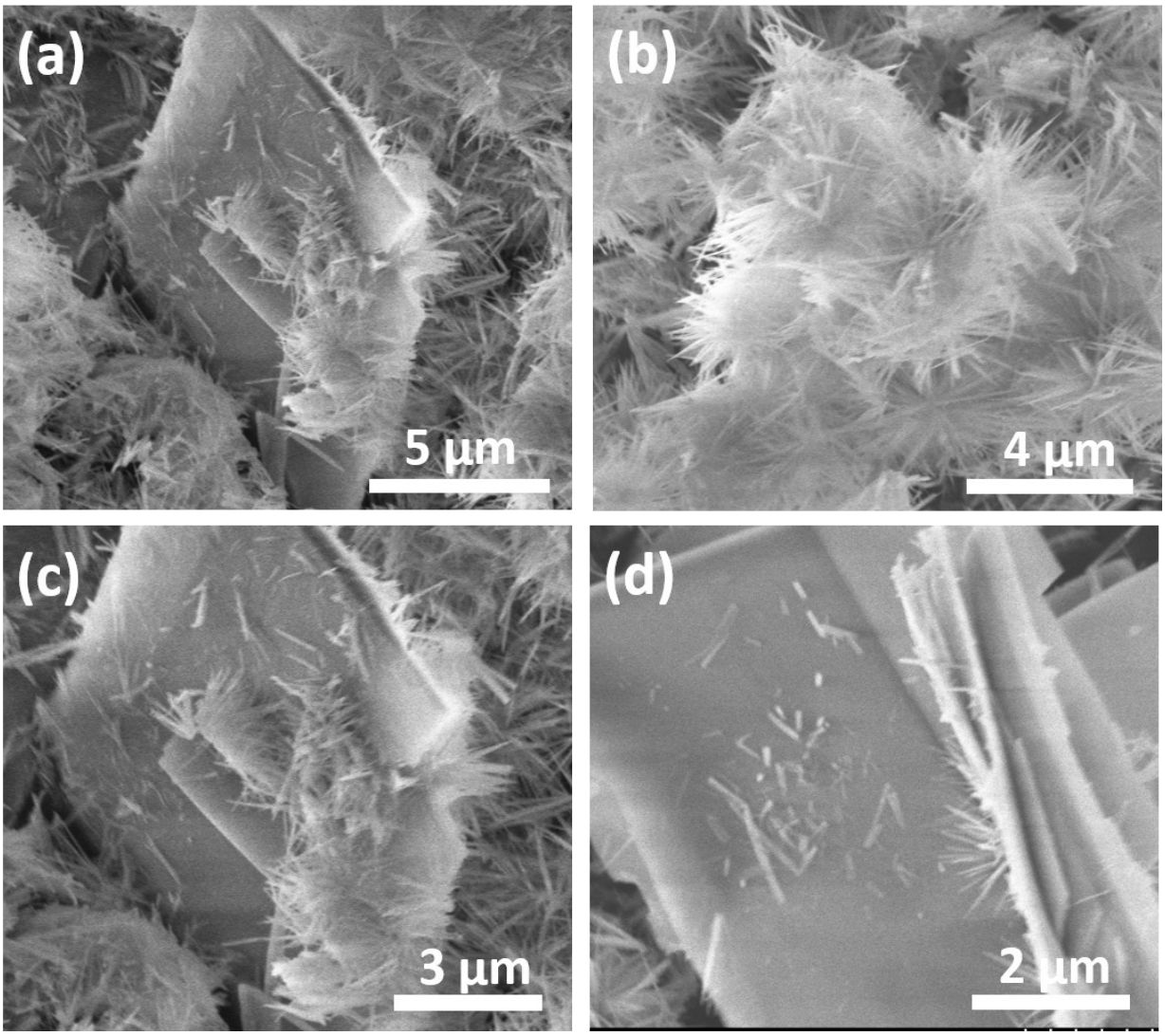

Fig. S3 Scanning Transmission Electron Microscopy images at reaction time equal to 3 hours for $Ni_xCo_{2-x}(CO)_3(OH)_2$

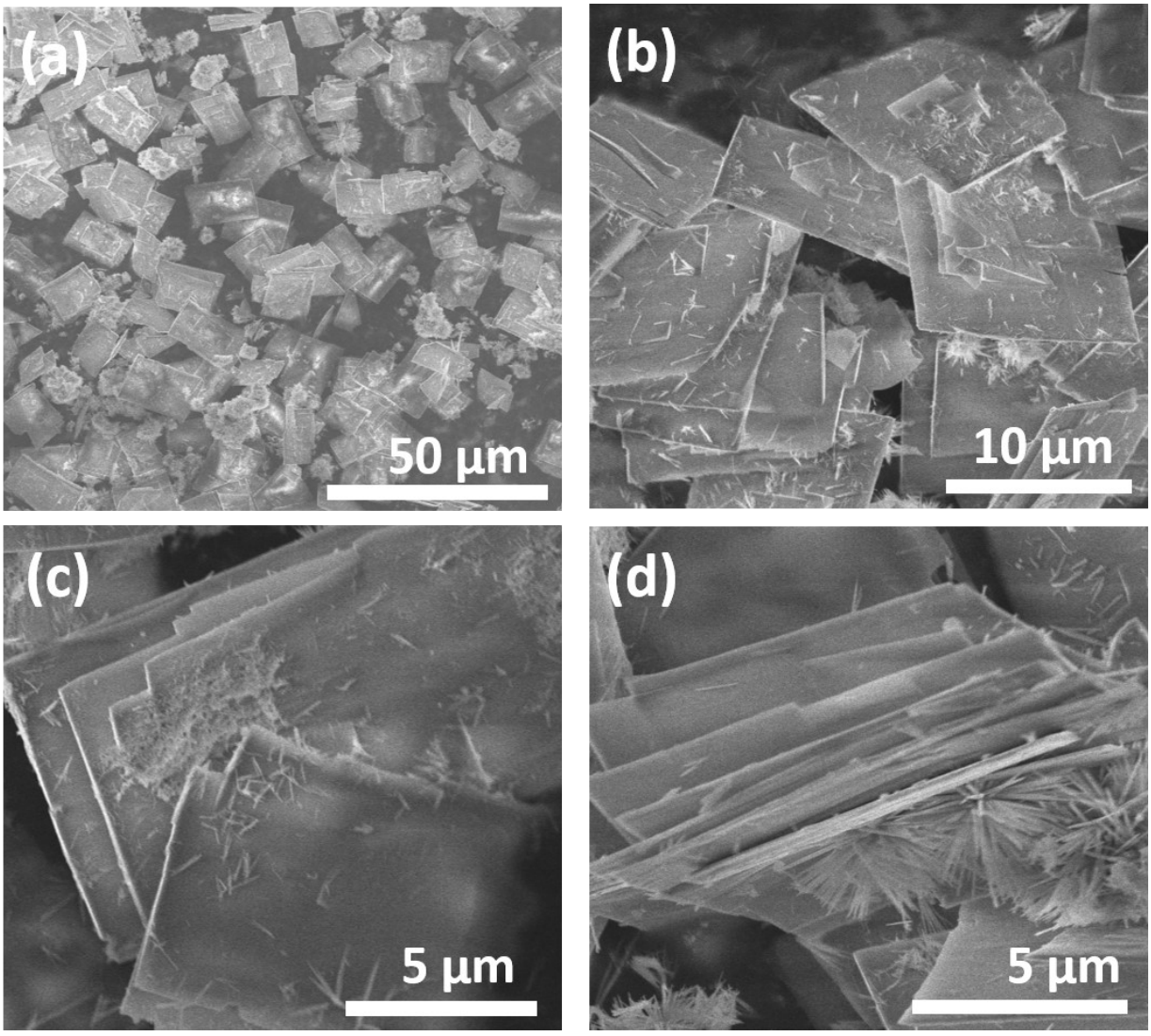

Fig. S4 Scanning Transmission Electron Microscopy images at reaction time equal to 4 hours for $Ni_xCo_{2-x}(CO)_3(OH)_2$

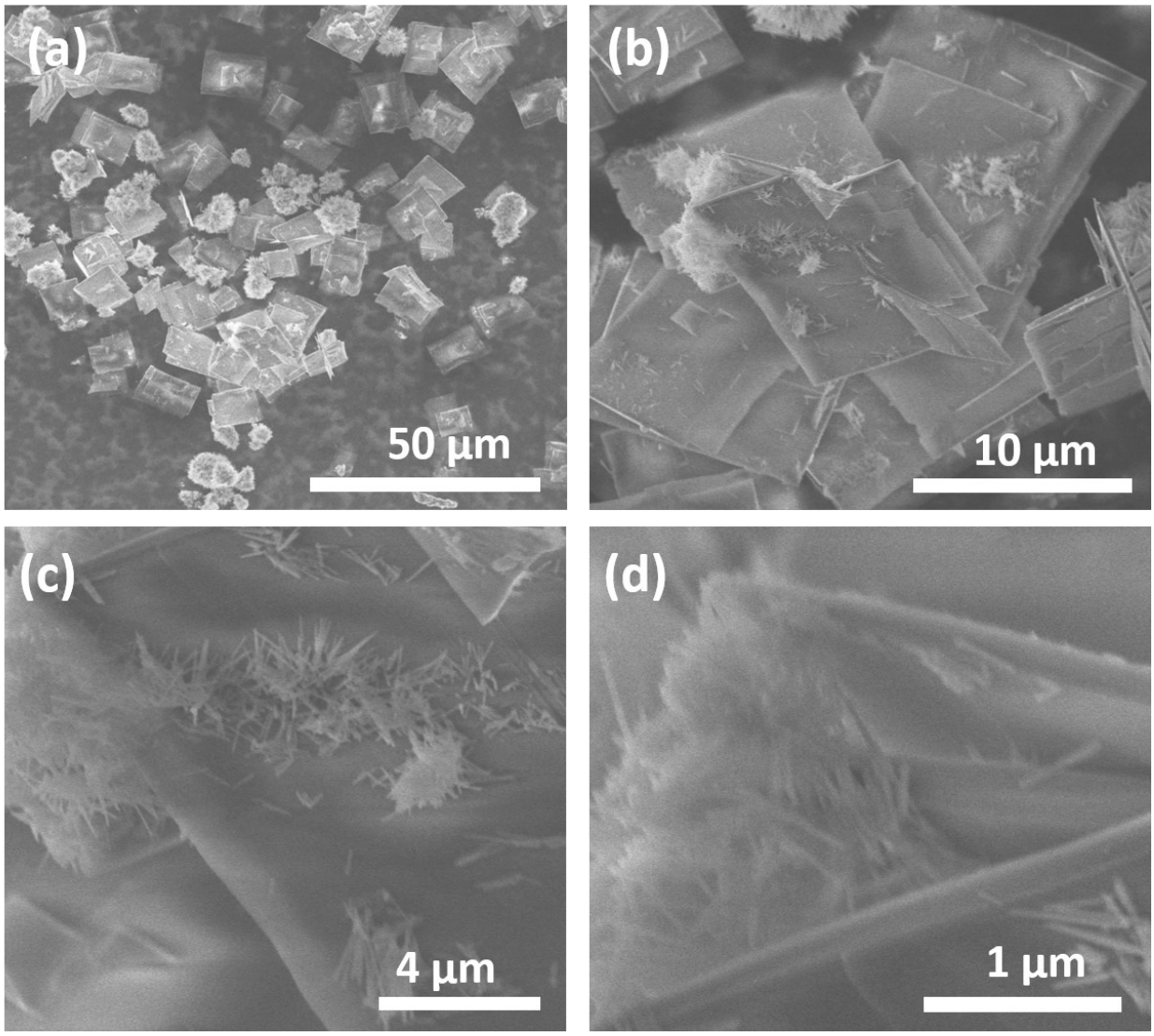

Fig. S5 Scanning Transmission Electron Microscopy images at reaction time equal to 5 hours for $Ni_xCo_{2-x}(CO)_3(OH)_2$

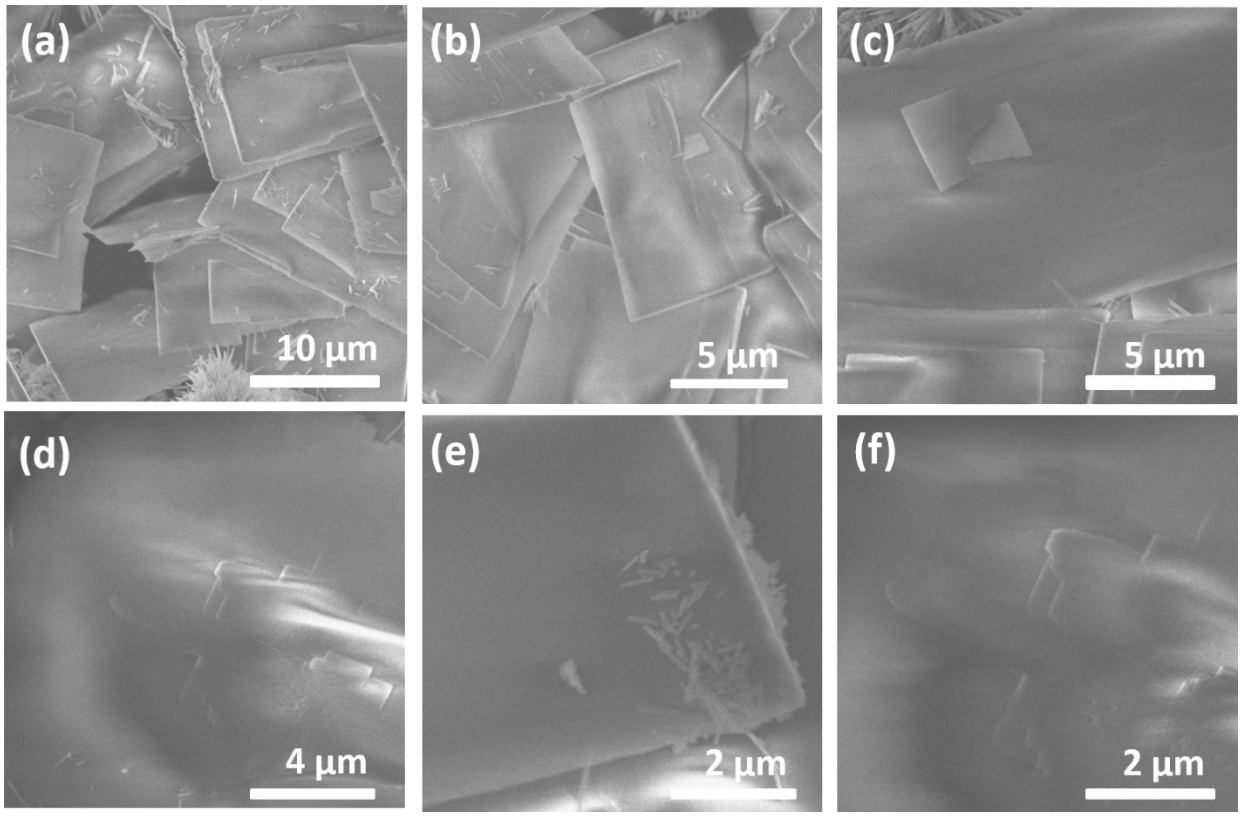

Fig. S6 Scanning Transmission Electron Microscopy images at reaction time equal to 6 hours for $Ni_xCo_{2-x}(CO)_3(OH)_2$

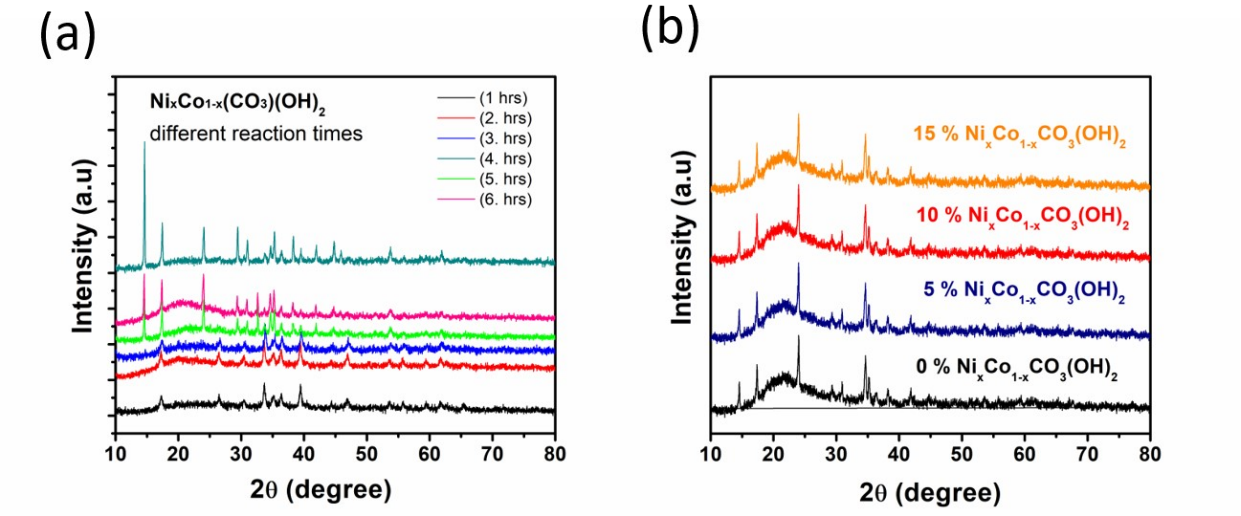

Fig. S7 (a) XRD patterns of all the products from 1 to 6 hours reaction time with 10 % Ni doping; (b) XRD pattern of different Ni doped hydroxide carbonates (Ni doping 0 to 15 %) 6 hours reaction

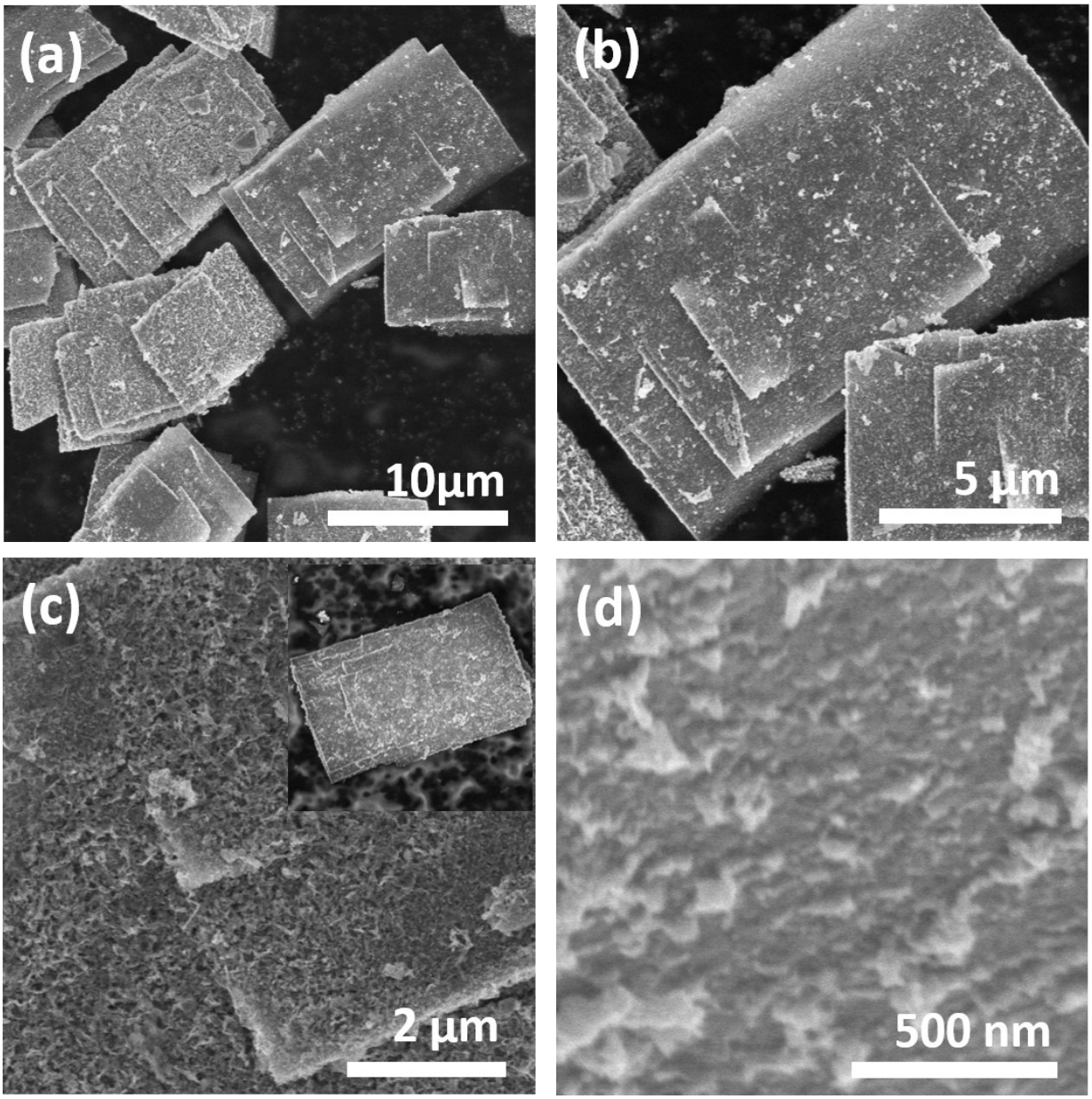

Fig. S8 Scanning Transmission Electron Microscopy images of 10 % Ni-doped $Co_{0.85}Se$, Selenization of 6h- $Ni_xCo_{2-X}(CO)_3(OH)_2$

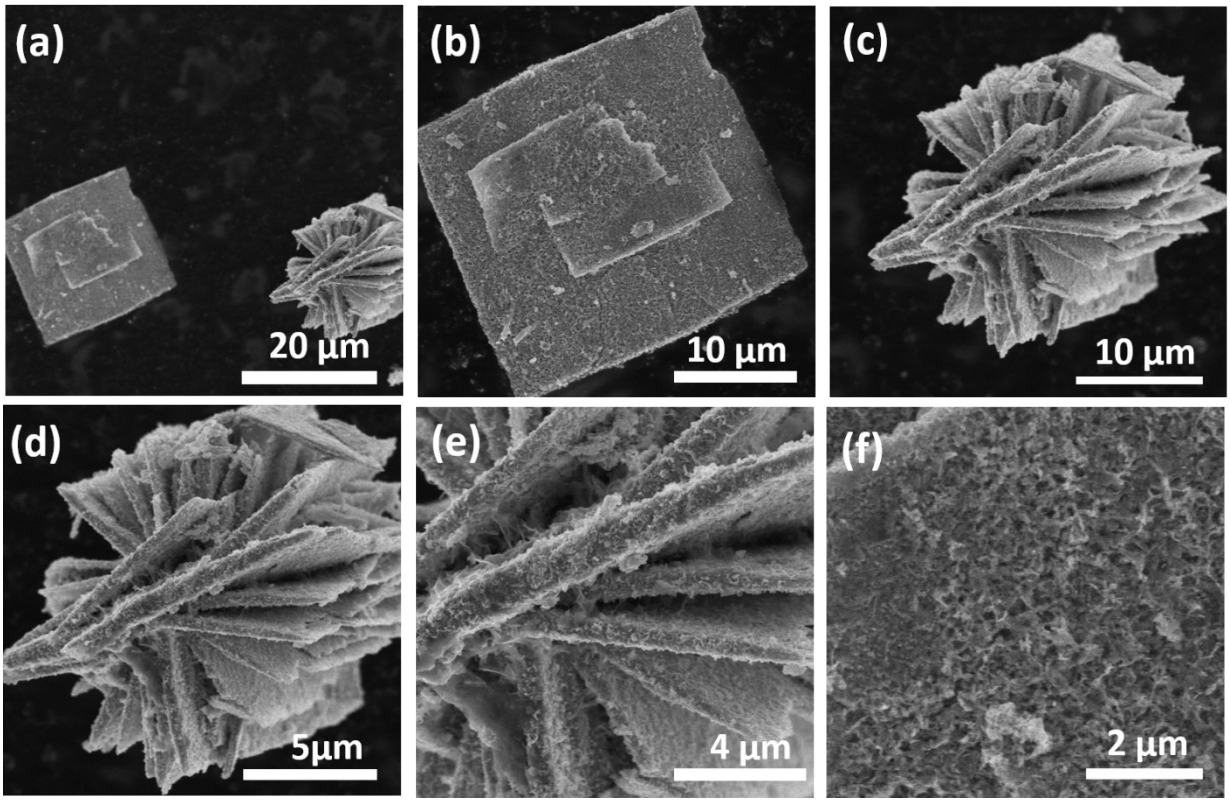

Fig. S9 Scanning Transmission Electron Microscopy images of $Co_{0.85}Se$, Selenization of 6 h- of $Co_2(CO)_3(OH)_2$

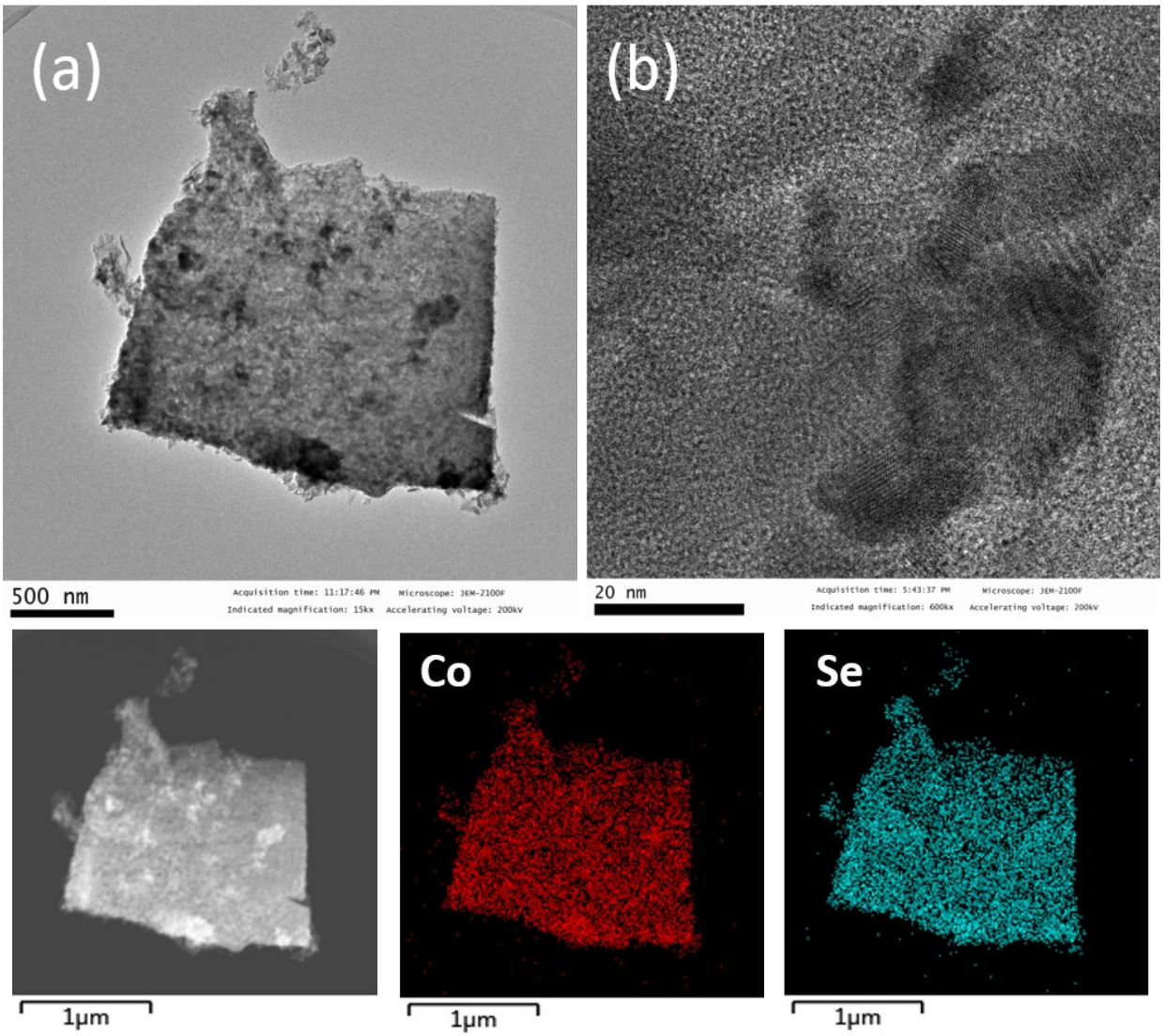

Fig. S10 Transmission Electron Microscopy images and EDS elemental mapping of $Co_{0.85}Se$

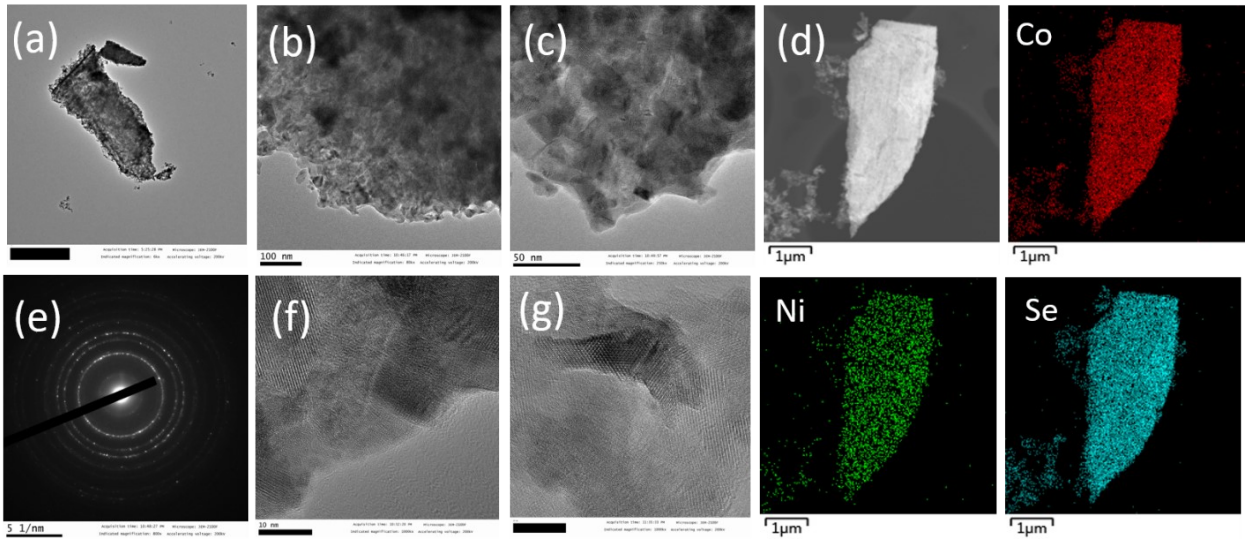

Fig. S11 Transmission Electron Microscopy images and EDS of 15% Ni-doped $(Ni,Co)_{0.85}Se$

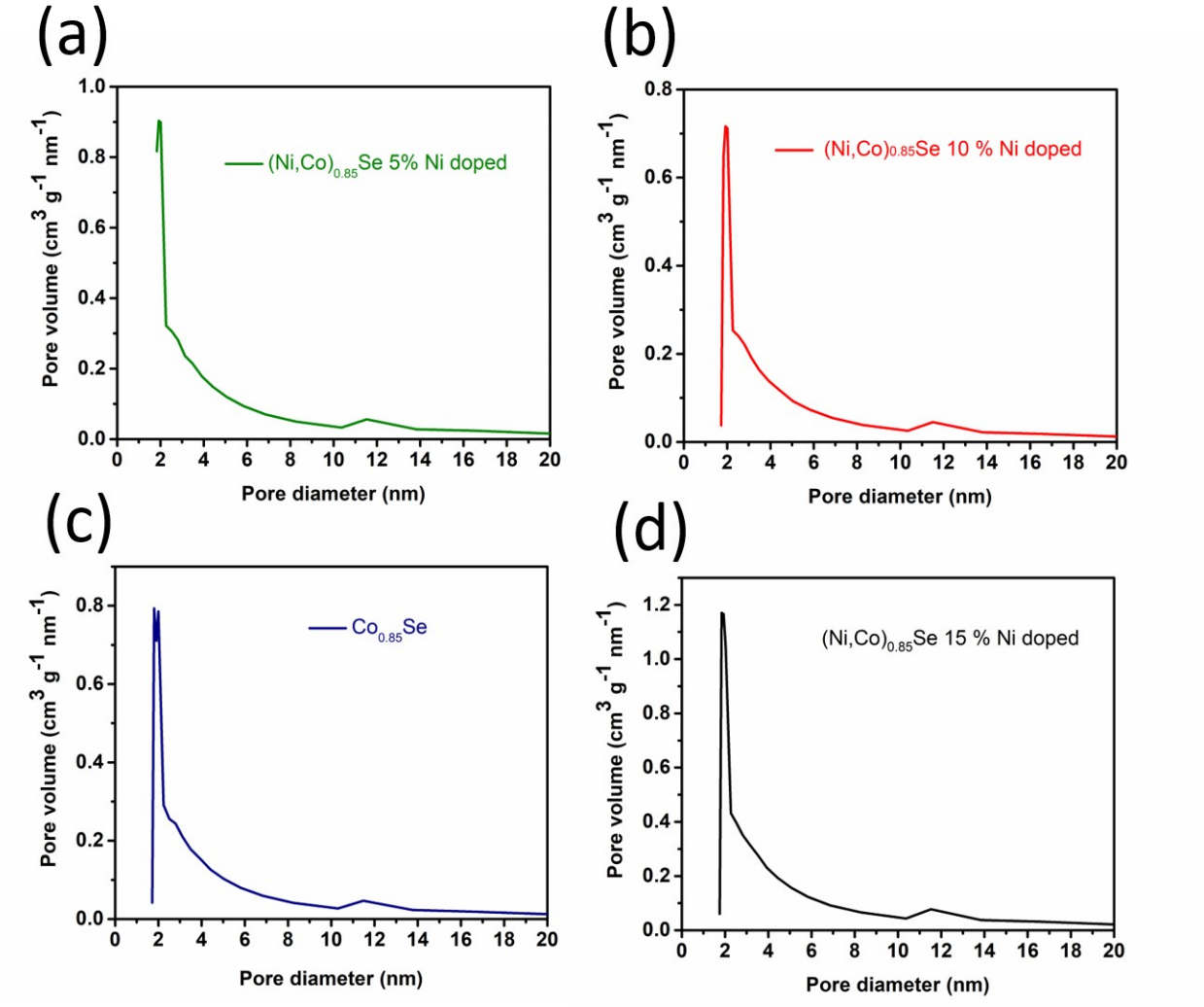

Fig. S12 Pore size distribution of $C_{o.85}Se$ and $(Ni, Co)_{0.85}Se$ samples

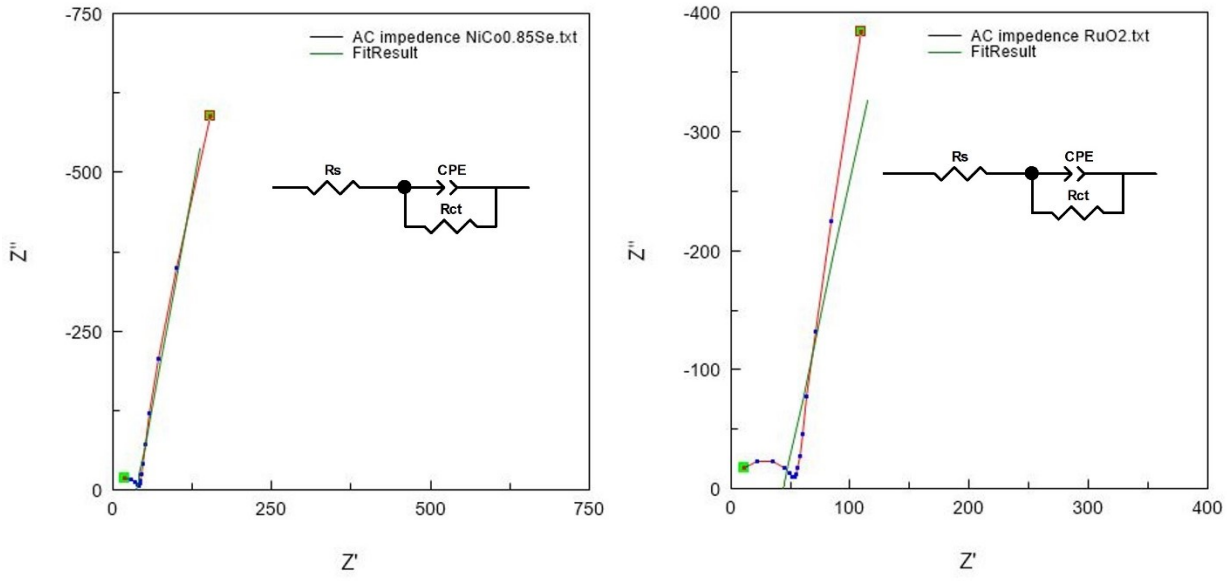

Fig. S13 The equivalent circuit of EIS spectra and corresponding fitting data

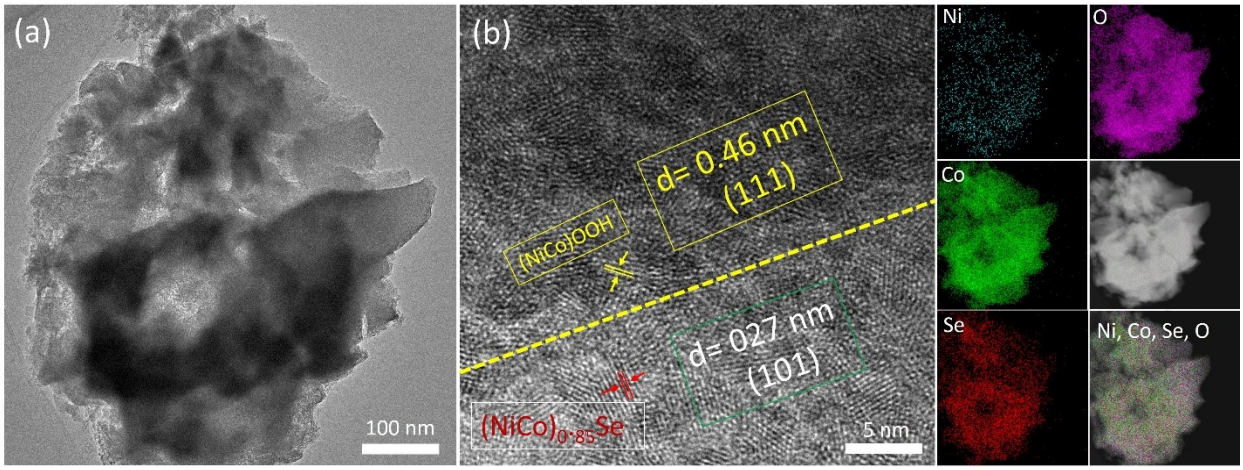

Fig. S14 Transmission Electron microscopy Image of the catalyst after 12 hrs of chronopotentiometry (a) Sheet structures (b) High resolution and Elemental mapping

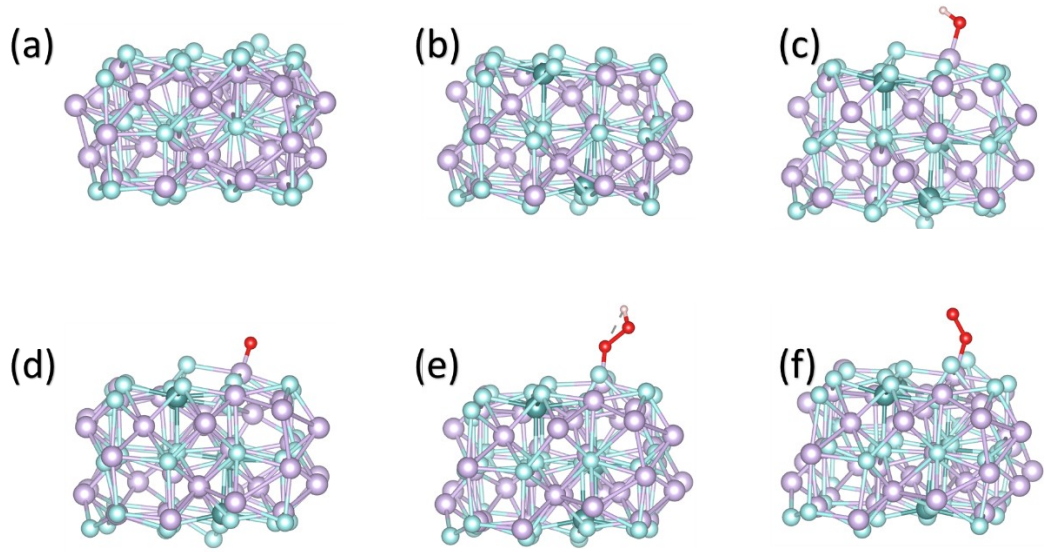

Figure S15 (a), (b), (c), (d), (e), (f) The Most stable structures of $Co_{0.85}Se$, $(Ni, Co)_{0.85}Se$, adsorbed OH, O, OOH and O_2, respectively.

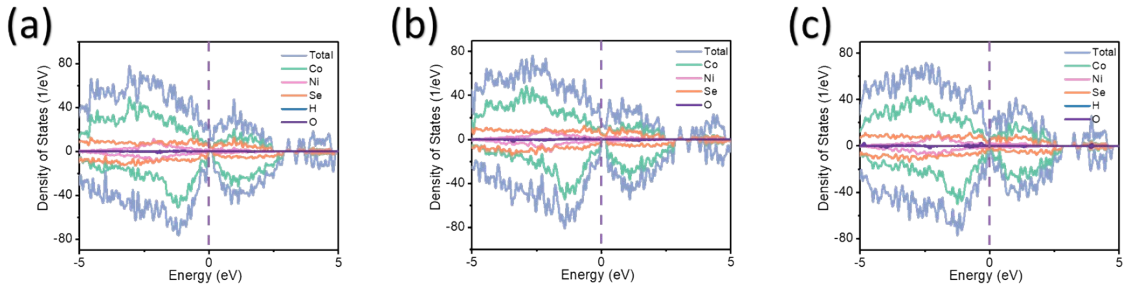

Figure S16 (a), (b), (c) DOS profiles of adsorbed *OH, *O, *OOH on$(Ni, Co)_{0.85}Se$, respectively

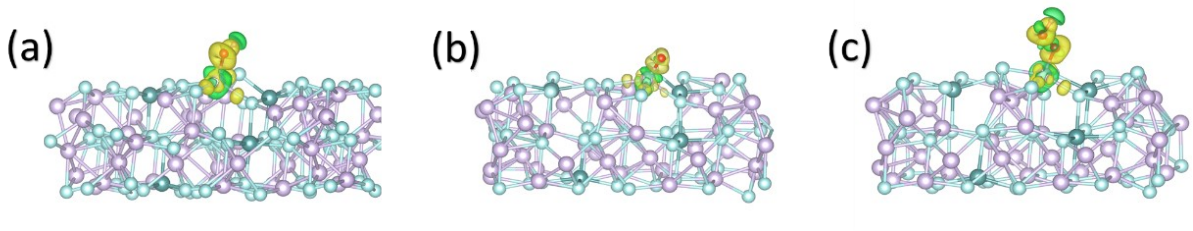

Figure S17 (a), (b), (c) charge density difference of adsorbed *OH, *O, *OOH on $(Ni, Co)_{0.85}Se$, respectively.

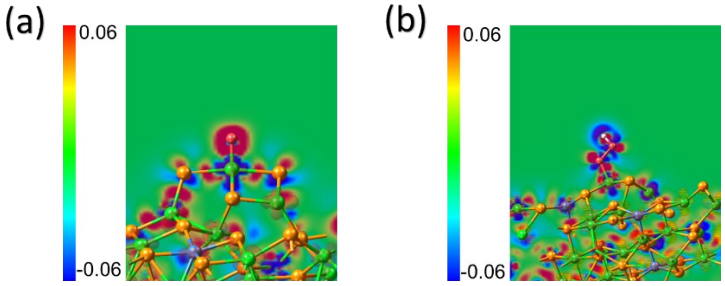

Figure S18 (a), (b), (c) 2D sectional views of charge density difference for adsorbed *O, *OOH on $(Ni, Co)_{0.85}Se$, respectively.

Author Contributions:

M.S. Riaz: conceptualization, supervision, writing original draft, and review and editing.
P. Farràs and F.Q. Huang: supervision, formal analysis, and review.
Qi Huang's theoretical investigation of DFT studies and formal analysis.
J. Duan and S. Chen supervise the theoretical studies.

References

1 M. S. Riaz, X. Yuan, Y. Zhao, C. Dong, S. Nong, Z. Ali and F. Huang, *Adv. Sustain. Syst.*, 2019, **3**, 1800167.
2 Z. Zhang, Z. Wang, S. He, C. Wang, M. Jin and Y. Yin, *Chem Sci*, 2015, **6**, 5197-5203.
3 A. Diez-Escudero, M. Espanol and M.-P. Ginebra, *Chem Sci*,, 2024, **15**, 55-76.
4 L. Ping, G. E. Minarik, H. Gao, J. Cao, T. Li, H. Kitadai and X. Ling, *Sci. Rep.*, 2024, **14**, 3817.
5 F. Sun, S. Wang, Y. Wang, J. Zhang, X. Yu, Y. Zhou and J. Zhang, *Sensors*, 2019, **19**, 2938.
6 G. Kresse and J. Furthmuller, *Comput. Mater. Sci.*, 1996, **6**, 15-50.
7 Kresse and Furthmuller, *Phys. Rev. B Condens.*, 1996, **54**, 11169-11186.
8 Perdew, Burke and Ernzerhof, *Phys. Rev. Lett.*, 1996, **77**, 3865-3868.
9 Perdew, Burke and Wang, *Phys. Rev. B Condens.*, 1996, **54**, 16533-16539.
10 Blochl, *Phys. Rev. B Condens.*, 1994, **50**, 17953-17979.
11 G. Kresse and D. Joubert, *Phys. Rev. B Condens.*, 1999, **59**, 1758-1775.
12 L. Yan, L. Xie, X.-L. Wu, M. Qian, J. Chen, Y. Zhong and Y. Hu, *Carbon Energy*, 2021, **3**, 856-865.
13 J. Feng, C. Yang, L. Zhang, F. Lai, L. Du and X. Yang, *Carbon Energy*, 2020, **2**, 614-623.
14 Y. Sun, B. Xia, S. Ding, L. Yu, S. Chen and J. Duan, *J. Mater. Chem. A*, 2021, **9**, 20040-20047.
15 X. Yuan, H. Ge, X. Wang, C. Dong, W. Dong, M. S. Riaz, Z. Xu, J. Zhang and F. Huang, *ACS Energy Lett.* 2017, **2**, 1208-1213.
16 X. Yuan, Z. Zhang, Z. Liu, X. Wang, C. Dong, M. S. Riaz and F. Huang, *Inorg. Chem. Front.,* 2018, **5**, 1844-1848.
17 X. Yuan, M. S. Riaz, X. Wang, C. Dong, Z. Zhang and F. Huang, *Chem. Eur. J.* 2018, **24**, 3707-3711.
18 M. S. Riaz, S. Zhao, C. Dong, S. Nong, Y. Zhao, M. J. Iqbal and F. Huang, *Chem. Eur. J.* 2020, **26**, 1306-1313.